Tribology Letters (2021) 69:96
https://doi.org/10.1007/s11249-021-01453-7

ORIGINAL PAPER

Structurally Driven Environmental Degradation of Friction in MoS_2 Films

John F. Curry[1] · Taisuke Ohta[1] · Frank W. DelRio[1] · Philip Mantos[1] · Morgan R. Jones[1] · Tomas F. Babuska[1,2] · N. Scott Bobbitt[1] · Nicolas Argibay[1] · Brandon A. Krick[2] · Michael T. Dugger[1] · Michael Chandross[1]

Received: 30 January 2021 / Accepted: 28 April 2021 / Published online: 22 June 2021

Abstract
We report an investigation of the friction mechanisms of MoS_2 thin films under changing environments and contact conditions using a variety of computational and experimental techniques. Molecular dynamics simulations were used to study the effects of water and molecular oxygen on friction and bonding of MoS_2 lamellae during initial sliding. Characterization via photoelectron emission microscopy (PEEM) and Kelvin probe force microscopy (KPFM) were used to determine work function changes in shear modified material within the top few nanometers of MoS_2 wear scars. The work function was shown to change with contact conditions and environment, and shown by density functional theory (DFT) calculations and literature reports to be correlated with lamellae size and thickness of the basally oriented surface layer. Results from nanoscale simulations and macroscale experiments suggest that the evolution of the friction behavior of MoS_2 is linked primarily to the formation or inhibition of a basally oriented, molecularly thin surface film with long-range order.

Keywords MoS_2 · Molecular dynamics · DFT · PEEM · KPFM · Friction mechanism · Crystallite size · Defects

1 Introduction

Molybdenum disulfide (MoS_2) films have been used as a solid lubricant in aerospace and related applications for more than 70 years [1–7] because they can exhibit extremely low friction and wear reduction in inert environments like the vacuum of space. The low shear strength and subsequently low friction coefficients of MoS_2 are a result of its lamellar structure, where basally oriented, molecularly thin lamellae with sulfur-terminated surfaces interact predominantly through weak van der Waals forces. Apart from its mechanical properties, MoS_2 has enjoyed renewed interest for its chemical and electrical properties with applications in areas such as catalysis [8, 9] and optoelectronics [10–12]. Recent studies have noted that the degradation in performance and stability of MoS_2 thin films in ambient conditions remains a challenge to practical utility in a wide range of applications [13–15]. A detailed physical/chemical understanding of how friction behavior in these films degrades (i.e., increased friction and wear) when exposed to water and other environmental contaminants, however, has remained elusive.

The tribological community has made significant progress in understanding the independent and combined roles of water and oxygen in this degradation in tribological performance over time (i.e., aging behavior) of MoS_2 contacts [16, 17]. Two predominant theories have emerged to explain the increase in shear strength of films exposed to ambient air at room temperature: (1) the formation of oxides through reactions with water and/or oxygen [18–22], and (2) adsorption of water [16, 23–29]. Khare and Burris recently showed that below a temperature threshold of 100 °C, higher friction in the presence of water vapor is likely associated either with the physisorption of environmental water or effusion from the bulk [16]. At temperatures above 100 °C, the presence of molecular oxygen resulted in oxidation and increased friction of the MoS_2 coating. Friction has also been shown to decrease upon annealing in inert atmospheres [16, 30], and to be recoverable after cycling from humid to dry environments [20, 23, 31], indicating that physisorbed water is a leading cause of the increased shear strength. However, a clear

✉ John F. Curry
jcurry@sandia.gov

[1] Material, Physical and Chemical Sciences Center, Sandia National Laboratories, Albuquerque, NM, USA

[2] FAMU-FSU College of Engineering, Florida State University, Tallahassee, FL, USA

mechanism linking water exposure to increased friction remains elusive. Proposed reasons include polar bonding between lamellae [27], capillary forces or enhanced adhesion [26, 32], among others. A complication arises for these theories in that water does not tend to intercalate between MoS_2 lamellae [33], and the basally oriented lamellae that accommodate shear during sliding tend to be mildly hydrophilic and become mildly hydrophobic when exposed to ambient hydrocarbons [34–37].

Interactions between water molecules and unterminated edges of MoS_2 lamellae have also been suggested as an impediment to low-strength shear [33]. In macroscale contacts, edges of MoS_2 lamellae at the surface are likely oxidized prior to testing, further enhancing interactions with water [15, 24, 38–40]. Previous work by our group showed that the surface microstructure (i.e., crystallite or lamellae size and thickness of the oriented layer) has a significant impact on friction behavior and its evolution in the presence of various vapor species, including water and molecular oxygen. In this paper, we present further evidence supporting the hypothesis that degradation in friction in humid environments is largely a result of changes in the surface microstructure due to water and oxygen exposure.

2 Materials and Methods

2.1 Deposition and Tribological Test Methods

MoS_2 thin films were prepared via direct current (DC) magnetron sputtering under 10 mTorr pressure of argon gas. High purity MoS_2 and Ti targets (Angstrom Sciences) were used to produce 650 nm thick MoS_2 films on top of a 75 nm Ti adhesion layer at 200 W and 300 W bias voltages on 1 cm^2 Si wafers. Separate samples were prepared for PEEM and KPFM analysis.

Tribological testing was conducted on a custom built linear-reciprocating microtribometer [41–43]. Unless otherwise noted, experiments were performed in a dry N_2-filled glovebox (< 10 ppm O_2 and < 10 ppm H_2O), using a chilled mirror hygrometer to measure humidity. Three test series were run on each sample, the first at a 200 mN load for 250 cycles in two different environments, one track in humidified (50% RH) N_2 and the other in dry N_2, the second at a constant 200 mN load in dry N_2 with variable cycle count (1, 10, and 250 cycles) and the third in dry N_2 for 250 cycles with varying load (10, 50, and 200 mN). All experiments used a 1 mm diameter ruby ball with a sliding speed of 1 mm/s. Wear scars were spaced in close proximity to each other to fit multiple tracks into the 2 mm diameter analysis window available to PEEM. This allowed for direct comparisons between tracks of a given set without re-adjusting the PEEM system.

2.2 Molecular Dynamics: Shear and Bonding Simulations

Molecular dynamics (MD) simulations with a reactive force field (ReaxFF) [44] were used to probe the interactions between molecular oxygen, water and triangular MoS_2 lamellae to investigate how adsorbed species induce structural changes and influence shear strength (and thus friction coefficient). Simulations consisted of three layers of randomly rotated lamellae (triangles ~ 3 nm on a side) of MoS_2 sandwiched between four monolayers of MoS_2. The outer layers were held rigid to apply normal load and shear. After initial shearing, the top layers of MoS_2 were removed, and the lamellae were exposed to oxygen or water at a pressure of 100 atm. These systems were equilibrated for 100 ps before atmospheric molecules were removed and the upper MoS_2 layers replaced for further shear. Simulation methods and schematic of the simulation structure can be found in a previous publication [45].

2.3 Density Functional Theory: Work Function Calculations of Lamellae

Work function of different size lamellae, monolayer and bulk MoS_2, were calculated with density functional theory (DFT). The Vienna Ab initio Simulation Package (VASP) v5.4.4 [46, 47] was used with the standard PAW_PBE pseudopotentials packaged with VASP (Mo: 08Apr2002 and S: 06Sep2000). The energy cutoff was 520 eV, equal to 1.3 times the largest ENMAX value for any of the pseudopotentials. The exchange correlation was treated with the PBE functional [48], and dispersion corrections were added using the DFT-D3 method from Grimme [49, 50] using Becke-Johnson damping. Gaussian smearing was employed with a sigma value of 0.05, and the k-points were treated using a $4 \times 4 \times 1$ Monkhorst–Pack grid [51]. Dipole corrections were used for the Z- direction (normal to the plane of MoS_2). The calculation was not spin polarized. The SCF convergence criterion was 10^{-4}, and structures were geometrically relaxed to a maximum force criterion of 0.02 eV/Å. VASP calculations were set up and managed using the Atomic Simulation Environment [52]. Integration was done with the "accurate" flag. The work function was computed using

$$\phi = E_{vac} - E_{Fermi} \quad (1)$$

where E_{vac} is the energy of the vacuum level and E_{Fermi} is the Fermi level from the VASP output. The vacuum energy is computed from a 1D averaged electrostatic potential based on the 3D potential output from VASP using the post-processing utility from Walsh and Catlow [53]. The bulk

layer calculations used 5 × 5 unit cells in the X and Y directions with at least 20 Å of vacuum space in the Z direction to avoid self-interaction.

2.4 KPFM Methods

KPFM measurements across wear scars were performed on a Bruker Dimension Icon atomic force microscope (AFM). The MoS_2 sample was mounted on a stainless-steel AFM puck and electrically grounded to the puck using silver paint. A dual-pass lift off was utilized on each line scan to obtain both surface height z and contact potential difference V_{CPD} data. On the first pass, z was measured via PeakForce Tapping, while on the second pass, V_{CPD} was measured by retracing the topography at a user-defined height and varying the DC sample voltage V_{DC} to null the cantilever oscillations ($V_{DC} = V_{CPD}$ when the tip-sample electrostatic force gradient was minimized). The work function of the sample ϕ_s was calculated from the V_{CPD} data through the relationship

$$\phi_s = \phi_t + eV_{CPD} \tag{2}$$

where ϕ_t is the work function of the tip and e is the elementary charge [54]. In this study, a single Bruker PFQNE-AL probe (nominal tip radius $R = 5$ nm, spring constant $k = 0.8$ N/m) was used to collect the z and V_{CPD} data for all of the wear scars, such that tip-to-tip variations in R and ϕ_t were mitigated. For this cantilever, k was taken to be the nominal value and ϕ_t was taken to be 4.88 eV from earlier work [55]. A Bruker PFKPFM-SMPL standard was imaged before and after the KPFM measurements; minimal changes in z and V_{CPD} across selected regions of the grating suggested that R and ϕ_t remained relatively constant throughout the experiments. The scan parameters were largely set by the ScanAsyst optimization technique; notable exceptions included a PeakForce setpoint of 10 nN and a lift-off height of 50 nm. A plane fit correction was applied to all z maps to account for sample tilt, while the V_{CPD} and ϕ_s maps were unprocessed. Cross-sectional profiles of the z and ϕ_s maps were taken across the widths of the wear scars, and the results presented herein were typical of data along the lengths of the wear scars.

2.5 PEEM Methods

PEEM measurements were conducted using a LEEM-III system (Elmitec Elektronenmikroskopie GmbH) coupled to a continuous-wave (CW), tunable wavelength light source based on a Xe lamp. The tunable wavelength light source was comprised of a pressurized Xe lamp (Energetiq, EQ-77 LDLS), a Czerny–Turner monochromator (Acton research, SP2150), and reflective refocusing optics, and illuminated the sample at an incident angle of 73° relative to the surface normal. Maps of the relative work function were determined by recording the photoelectron intensity as a function of the electron kinetic energy using monochromatic light illumination (185 nm wavelength, 6.70 eV) [56]. Similar to conventional analysis of X-ray photoelectron spectroscopy (XPS) and ultraviolet photoelectron spectroscopy (UPS) spectra, lines were fit to the low electron kinetic energy edge and the intersects of the fitted lines with the baseline of the spectra were determined. These intersects specified the locations of the vacuum level. The energy resolution of our electron energy filter was set to ~ 0.1 eV, which resulted in a total broadening of the spectral width by ~ 0.15 eV. This broadening due to the measurement resolution was corrected for post facto by shifting the edges of the spectra, similar to the procedure outlined in Yi et al. [57]. Maps of the vacuum level were obtained by fitting the spectra at each pixel. Local variation in the vacuum level across the field of view yielded the work function variation.

3 Results

3.1 Simulation Results from MD/DFT

Slices from MD simulations through the plane of lamellae sheared between periodic MoS_2 lamellae are shown in Fig. 1a–d. Lamellae with edge sites that are fully passivated with sulfur atoms are defect-free but non-stoichiometric; these are referred to as defect-free throughout the manuscript. Those where stoichiometry is preserved by removal of selective sulfur atoms from the edges of the lamellae are not fully passivated, and therefore defective and referred to as such.

Stoichiometric (defective) lamellae sheared in vacuum (i.e., no water or oxygen present, Fig. 1b) exhibited the highest friction coefficients, with $\mu \sim 0.15$ (Fig. 1e). The simulations show that lamellae tend to anchor themselves at random to neighboring lamellae because of the highly reactive exposed edges. This is likely the atomic scale process that is operative at the interface early in sliding during macroscale experiments when friction is observed to be high. Results from simulations where lamellae were exposed to water and molecular oxygen (Fig. 1c, d) showed lower friction than the defective lamellae, $\mu \sim 0.12$ and 0.07, respectively, likely because of passivation of exposed Mo atoms at the edges of lamellae by adsorbed species. This effect is visible in Fig. 1d. These simulations demonstrate that water tends to agglomerate at edges more than molecular oxygen.

To isolate and independently determine the effects of water and oxygen on the friction (i.e., without the changes in passivation of edge sites), we compare friction coefficients between defective and defect-free systems (i.e., with fully passivated, sulfur-terminated lamellae). As shown in

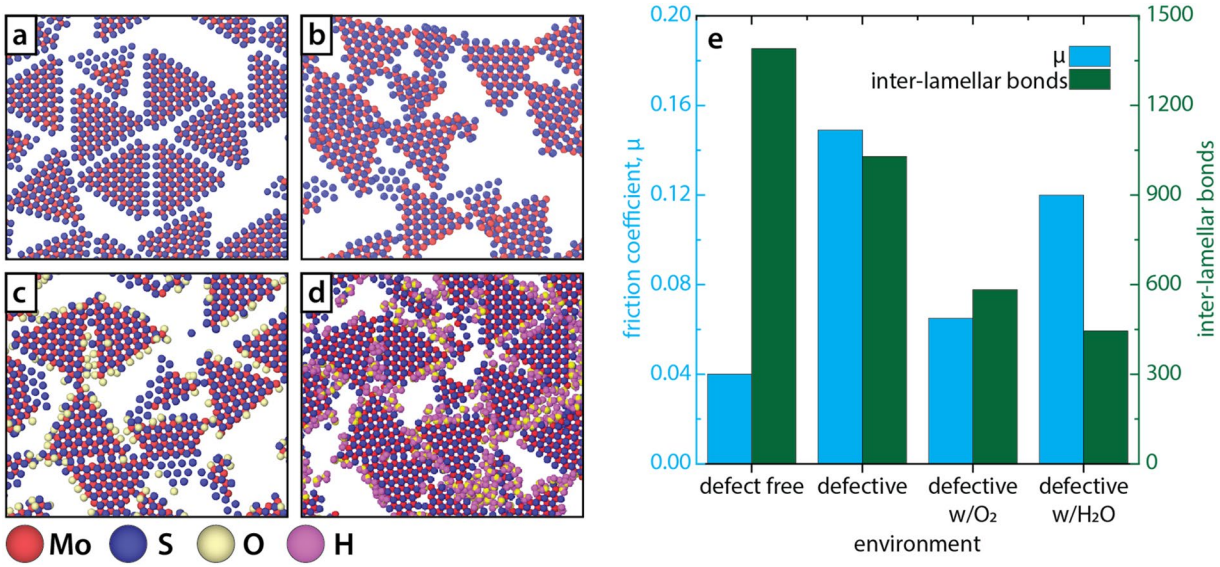

Fig. 1 Representative top-down cross-section view of simulation showing MoS_2 lamellae interactions for **a** defect-free lamellae, **b** defective lamellae, **c** defective lamellae with oxygen and **d** defective lamellae with water. Mo atoms are shown in red, S in blue, O in yellow and H in magenta. Friction coefficients from simulations and count of inter-lamellar interactions are shown in **e**

Fig. 1e, the defect-free systems exhibited the lowest friction coefficients. The effects of environmental species on microstructure evolution can be probed by counting the number of inter-lamellar bonds in all systems. While individual lamellae are held rigid so that no chemical reactions can occur, the lamellae are able to physisorb and form larger lamellar structures; we refer to these inter-lamellar interactions as bonds and quantify them through the atomic separation between different lamellae. The defect-free systems showed the highest number of inter-lamellar bonds, followed by the defective systems, and then defective systems exposed to water and molecular oxygen. This again indicates passivation from environmental species. Visualization of slices through the simulation box corroborate these results and show that under shear, lamellae order and begin to form larger lamellar structures.

3.2 Tribological Testing Results

Friction experiments in different environments (dry N_2 vs 50% RH N_2) were used to validate simulation results (Fig. 2a). Additional experimental parameters, including load and cycle count, were systematically varied to determine their impact on the evolution of the surface microstructure by producing surfaces that could be characterized with PEEM and KPFM.

Baseline experiments in dry N_2 using contact forces of 10, 50 and 200 mN exhibited friction behavior typical of MoS_2 films with high initial (few cycle) friction coefficients, $\mu \sim 0.1$–0.2, that gradually decreased throughout the first few hundred sliding cycles to values of $\mu \sim 0.05$. As in prior literature [58], these MoS_2 films obeyed Hertzian contact mechanics, with friction coefficients that were inversely proportional to contact force. Experiments in humid N_2 consistently led to higher friction than those in dry N_2 (Fig. 2a).

3.3 Work Function Measurements via PEEM/KPFM

The work function was measured by PEEM and KPFM on separate wear tracks for which representative friction data are shown in Fig. 2. Results of these analyses are shown in Figs. 3 and 4, respectively, where PEEM data are presented in terms of the relative change in work function from the as-deposited surface and KPFM data are presented as absolute values. The work function of these films was independently determined to be 4.9 eV from separate ultraviolet photoelectron spectroscopy (UPS) measurements, matching the values found via KPFM and corroborating the assumed value for the work function of the KPFM tip. PEEM and KPFM results were in good agreement and showed that the shear modified surfaces exhibit a higher work function than the as-deposited films by about 0.10–0.25 eV. The debris surrounding the wear scars,

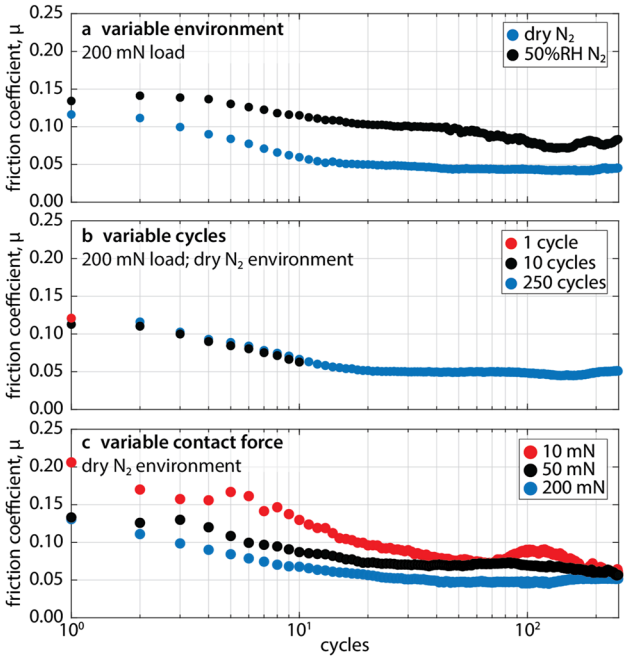

Fig. 2 Cycle average friction coefficients for experiments using a 1 mm diameter ruby ball and 1 mm/s sliding speed showing the impact of changing (**a**) environment (dry N_2 vs 50% RH N_2), **b** cycle count (1, 10, 250 cycles) and **c** contact force (10, 50, 200 mN)

conversely, shows a decrease in work function by a similar magnitude (0.10–0.25 eV) relative to the as-deposited film. Work functions increased with sliding cycles and were higher for friction experiments in dry N_2 than in humid N_2. Changes in work function as a function of normal force were less distinct, but local increases in work function appear to correlate with regions of increased peak contact pressure and were overall higher for the highest contact force. It should be noted that PEEM analysis was carried out in ultrahigh vacuum (UHV) while KPFM was conducted in laboratory air, but these differing analysis environments do not appear to have had an appreciable impact on results.

DFT was used to calculate changes in the work function of MoS_2 as a function of lamellae size and layer thickness, and we compare these results to prior literature as well as our PEEM and KPFM results. The work function for stochiometric lamellae ($Mo_{21}S_{42}$, $Mo_{28}S_{56}$ and $Mo_{36}S_{72}$) was found to increase with increasing lamella size from 4.79 eV to 5.02 eV. These values are smaller than that for a continuous monolayer of MoS_2 (5.69 eV), and the work function further increases to 5.94 eV for both 3- and 4-layer systems (Fig. 5), suggesting convergence to the bulk value. These results are in reasonable agreement with other DFT-calculated values for MoS_2 [59, 60].

4 Discussion

The results of the MD simulations suggest that the presence of water and molecular oxygen tend to interrupt interactions between lamellae, preventing formation of the multilayer, persistent basally oriented films that are associated with low friction in MoS_2 lubricated contacts. The formation of a basally oriented film with long range order is an important part of the run-in process for MoS_2 coatings and is frequently observed in initially amorphous PVD sputtered films [61, 62]. Previous studies on impinged MoS_2 films reached similar conclusions and suggested that films with ordered surface microstructures were less affected by humidity than amorphous films [29].

A key limitation of the simulations was the inability to directly simulate the restructuring of small lamellae during run-in, yet defective and defect-free simulations draw parallels to experimentally observed behaviors. For example, in simulations, defective lamellae readily anchor themselves at random to neighboring lamellae due to the highly reactive edges (Fig. 1b), analogous to run-in. The complete passivation of edges with sulfur (Fig. 1a) enables the lamellae to freely assemble themselves, in this case into larger ordered lamellae that exhibit low friction, similar to what is observed experimentally after a film is run-in [61, 62]. Interestingly, when exposed to water and oxygen, these simulations exhibit friction coefficients that agree well with experimental results [17]. Practically, however, the surface of sputtered MoS_2 films exposed to air are expected to be fully terminated, for example by oxygen (i.e., MoO_2, MoO_3). This is not likely a concern when comparing to simulation results, as wear during the first few cycles of sliding has been shown to remove the oxidized surface film, eventually leading to a recovery of low friction by the formation of ordered films and transfer films on the countersurface [45, 63]. This behavior is different from edges terminated by sulfur atoms, as oxides are also more likely to attract environmental contaminants like water [24, 25, 40].

Historically, transmission electron microscopy (TEM) or scanning tunneling microscopy (STM) has been used to quantify the density of in-plane defects like sulfur vacancies for monolayer MoS_2 films [12, 64, 65]. Unfortunately, these techniques tend to be labor-intensive and not well-suited for analysis of edge defects amongst multiple lamellae or the

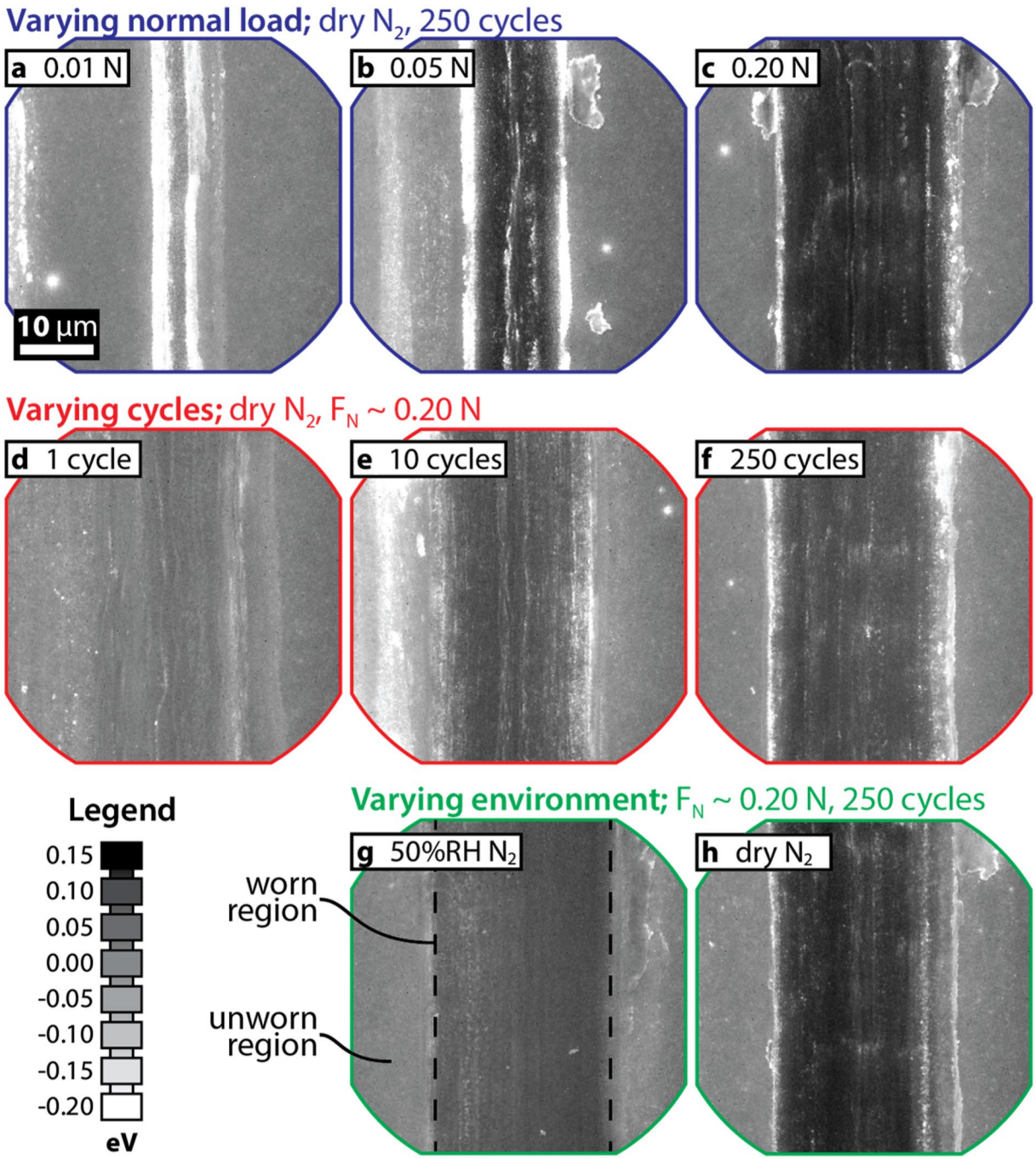

Fig. 3 Grayscale maps of relative work function change in eV from PEEM measurements of selected wear tracks shown in Fig. 2 as a function of **a–c** contact force for fixed number of cycles, **d–f** cycle count at fixed contact force, and **g–h** environment with fixed cycle count and normal force. Field of view is 50 µm across the diagonal direction of the images

rough surfaces typical of those created during macroscale sliding contact. Traditional X-ray diffraction (XRD) as well as the more surface sensitive grazing incidence techniques have been used to measure lamellae size in MoS_2 powder samples and thin films, but are not suited to the assessment of lateral dimensions of MoS_2 flakes, since calculated lamellae sizes are more representative of the thickness of the lamellar structure [66–68]. Raman spectroscopy has been used recently to assess defect density as well as lamellae size in MoS_2 [68–70], but again with limited depth-resolution.

Validation of simulation results in the present work was possible through techniques that allow for characterization of the chemical potential of wear scar surfaces (i.e., work function) that can help to infer defect density, lamellae size

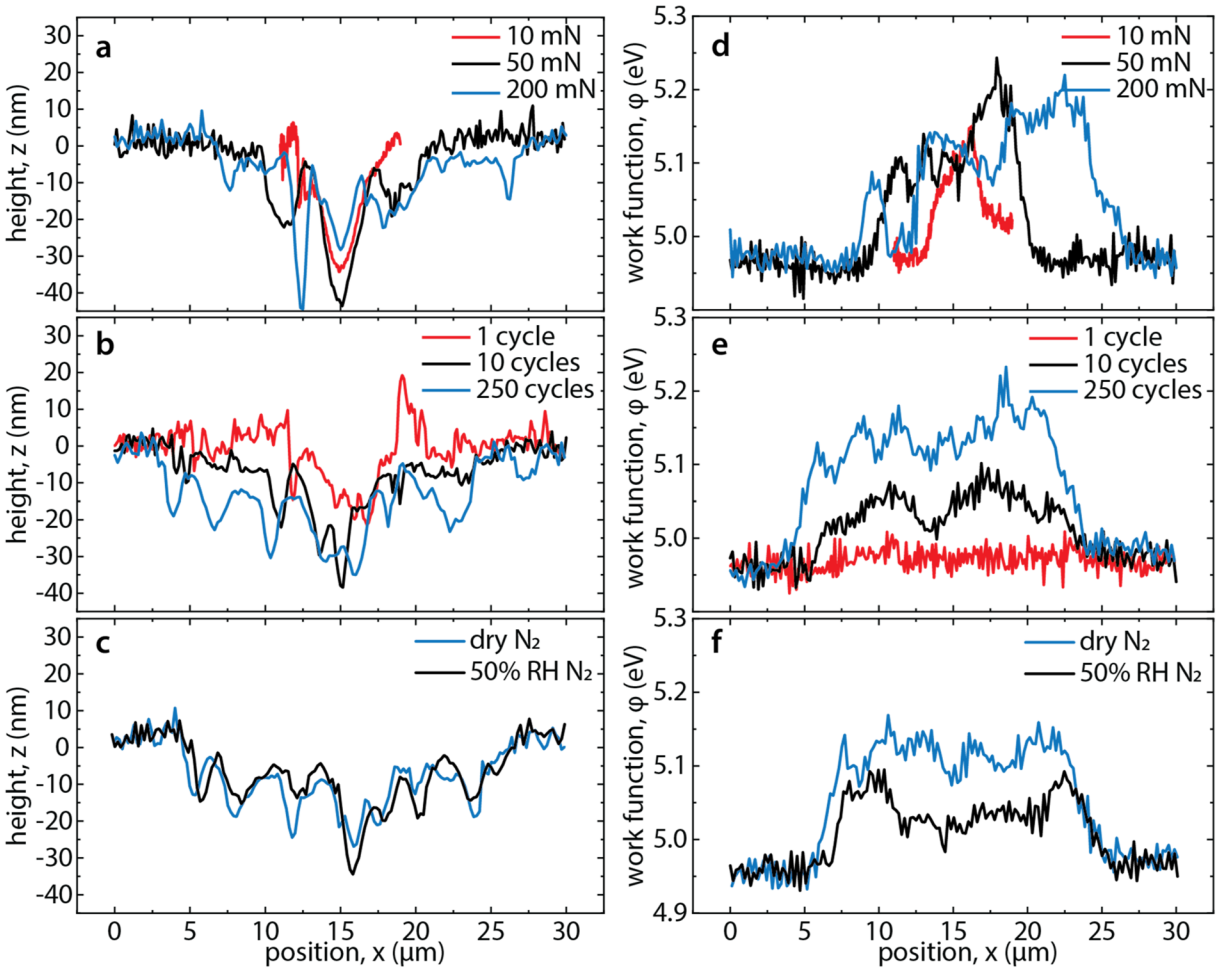

Fig. 4 **a–c** Cross-sectional topographical line scans and **d–f** corresponding work function in eV from KPFM measurements of selected wear tracks shown in Fig. 2 as a function of **a**, **d** contact force for fixed number of cycles, **b**, **e** cycle count at fixed contact force, and **c**, **f** environment with fixed cycle count and normal force

and thickness of the basally oriented layer (typically < 10 nm [61, 62]). The combination of PEEM and KPFM enabled a quantitative approach to characterize structural differences in the first few monolayers of macroscale wear tracks through measurements of work function at the surface. There have been several recent reports that show how the work function of single and multilayer MoS_2 systems are influenced by strain/defect density [71], oxidation state [72, 73], layer thickness and adsorbates [74, 75], as well as how work function varies across the surface of lamellae from edge to center [76, 77]. Generally, most of these factors increase the work function of MoS_2. For example, the work function of MoO_3 is typically 2 eV higher than that of MoS_2, well above the measured increase of 0.1–0.25 eV observed in the wear scars in our experiments. It is unlikely that there is an appreciable amount of oxidation at the surface of the wear scar [45], and it is more likely to find MoO_3 in the surrounding as-deposited film, but as others have shown, these films do not typically undergo appreciable oxidation during storage in dry N_2 [38]. Lastly, adsorbates are not thought to play an appreciable role in our results, as PEEM was performed in UHV and KPFM in lab air, and results from both are in good agreement.

This work shows that size and thickness of the lamellar structures in the wear tracks, and the presence of edge sites were the main factors contributing to the observed changes in work function and friction behavior in this investigation. As mentioned previously, MoS_2 films gradually form a thin (~ 10 nm) basally oriented layer at the sliding interface during the first few cycles of sliding [61, 62]. Notably, the work function difference between single layer and bulk MoS_2 films has been shown to be approximately 0.10–0.25 eV [74, 75], identical to the difference in values between the as-deposited regions, and the wear tracks that showed low steady-state friction. This layer dependence is best exemplified in the cycle-resolved results for PEEM and KPFM,

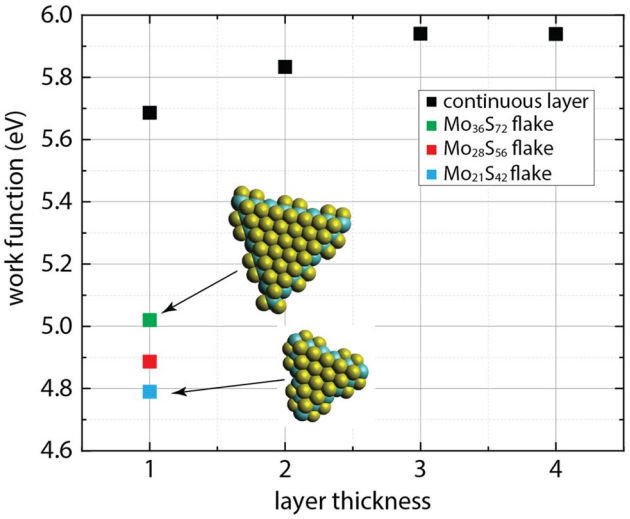

Fig. 5 DFT calculations of the work function of MoS_2 lamellae for monolayer lamellae of increasing size and continuous MoS_2 lamellae with increasing layers. Here, Mo atoms are shown in cyan and S in yellow

(Figs. 3d–f and 4b, e) where the work function was shown to gradually increase as the relatively thick, effectively bulk, film is run in and the thickness of the oriented surface film increased. These results are also supported by our DFT calculations (Fig. 5).

Other recent KPFM studies have shown that the edges and grain boundaries of MoS_2 monolayers (and other transition metal dichalcogenides) tend to exhibit lower voltage potentials [76, 77], and subsequently lower work functions as shown in Eq. 2. This relationship is also borne out in our DFT calculations, where smaller lamellae exhibit lower work functions (4.79 eV) than larger lamellae (5.02 eV), and both are lower than the work functions of continuous monolayers and bulk MoS_2 (5.69–5.94 eV, Fig. 5). This implies that work functions will increase with lamellar dimensions inside wear scars. We observe this relationship in our experiments in dry N_2, but not humid N_2. These experimental results corroborate trends observed in simulations showing that water prevents coalescence of small lamellae and their assembly into larger lamellae, ultimately resulting in higher friction coefficients (Fig. 1). In addition, debris around the edges of the wear tracks likely consists of smaller or thinner crystallites than those found inside the contact zone, because of the shorter contact times for debris ejected from the contact, as shown in Fig. 3, and this debris has lower work functions than the wear scars.

While the use of work function measurements is a promising technique to quantify differences between the surface microstructure in macroscale contacts, more work is necessary to confirm these hypotheses. Specifically, future investigations will focus on linking work function to structural characteristics of monolayer MoS_2 systems, and how these are correlated to structures observed in the few monolayer surface films generated during macroscale sliding contact.

5 Conclusions

A combination of simulations, experiments, and characterization techniques were used to elucidate the fundamental mechanisms responsible for the friction behavior for MoS_2 films in humid and oxygenated environments. MD simulations showed that exposure to water and molecular oxygen impacts the inter-lamellar interactions and ordering of MoS_2 lamellae under shear, interrupting the formation of larger lamellae and increasing friction coefficients over those of less reactive, edge-terminated lamellae.

Macroscale sliding contact experiments and ex situ characterization were used to corroborate simulations results. Specifically, changes in the work function in wear tracks were measured using KPFM/PEEM and correlated to microstructural changes as a function of changes in contact force and cycle count, both in dry and humid N_2. This approach enabled the first detailed, highly spatially-resolved analysis of macroscale contacts on thick (> 1 µm) physical vapor deposited (PVD) films with shear modified layers on the order of ~ 1% of the film thickness. This analysis is typically out of the reach of traditional methods for probing microstructure and defect densities (e.g., Raman, TEM, XRD). Work function changes on the surface of MoS_2 wear tracks suggest that the lamellae size and thickness of basally oriented material are strongly influenced by the presence of contaminants that effectively restrict coalescence and formation of larger, ordered MoS_2 lamellae. This directly prevents the transition to the desirable low friction state. Further work is necessary to develop quantitative characterization techniques to accurately probe changes in surface microstructure for the thicker films representative of running contacts. Ultimately, understanding the effects of environmental species on the microstructure of MoS_2 coatings can enable tailoring of the surface microstructure to mitigate the detrimental effects of long- and short-term aging and degradation.

Acknowledgements The authors are grateful to Michael Walsh of Honeywell's Kansas City National Security Campus for deposition of the sputtered MoS_2 films, and Samantha Gayle Rosenberg of Sandia National Laboratories for the UPS measurement. This work was funded by the Laboratory Directed Research and Development (LDRD) program at Sandia National Laboratories, a multi-mission laboratory managed and operated by National Technology and Engineering Solutions of Sandia, LLC., a wholly owned subsidiary of Honeywell International, Inc., for the U.S. Department of Energy's National Nuclear Security Administration under contract DE-NA0003525. The PEEM/KPFM operation was, in part, supported by Center for Integrated Nanotechnologies user program, an Office of Science User Facility operated for the U.S. Department of Energy (DOE) Office of Science

(DE-AC04-94AL85000). Any subjective views or opinions that might be expressed in the paper do not necessarily represent the views of the U.S. Department of Energy or the United States Government.

References

1. Bell, M.E., Findlay, J.H.: Molybdenite as a new lubricant. Phys. Rev. **59**, 922 (1941)
2. Godfrey, D., Nelson, E.C.: Oxidation characteristics of molybdenum disulfide and effect of such oxidation on its role as a solid-film lubricant. https://core.ac.uk/download/pdf/42803573.pdf (1949)
3. Peterson, M.B., Johnson, R.L.: Friction and wear investigation of molybdenum disulfide II: effects of contaminants and method of application. https://ntrs.nasa.gov/archive/nasa/casi.ntrs.nasa.gov/19930083852.pdf (1954)
4. Fusaro, R.L.: Lubrication and failure mechanisms of molybdenum disulfide films. 1: Effect of atmosphere. http://ntrs.nasa.gov/search.jsp?R=19790004987 (1978)
5. Fusaro, R.L.: Lubrication and failure mechanisms of molybdenum disulfide films. 2: Effect of substrate roughness. https://ntrs.nasa.gov/search.jsp?R=19790004988 (1978)
6. Fleischauer, P.D., Hilton, M.R.: Applications of space tribology in the USA. Tribol. Int. **23**, 135–139 (1990)
7. Fusaro, R.L.: Lubrication of Space Systems. https://ntrs.nasa.gov/search.jsp?R=19970003296 (1995)
8. Byskov, L.S., Nørskov, J.K., Clausen, B.S., Topsøe, H.: Edge termination of MoS_2 and CoMoS catalyst particles. Catal. Lett. **64**, 95–99 (2000)
9. Kooyman, P.J., Rob van Veen, J.A.: The detrimental effect of exposure to air on supported MoS_2. Catal. Today **130**, 135–138 (2008)
10. Radisavljevic, B., Radenovic, A., Brivio, J., Giacometti, V., Kis, A.: Single-layer MoS_2 transistors. Nat. Nanotechnol. **6**, 147–150 (2011)
11. Lopez-Sanchez, O., Lembke, D., Kayci, M., Radenovic, A., Kis, A.: Ultrasensitive photodetectors based on monolayer MoS_2. Nat. Nanotechnol. **8**, 497–501 (2013)
12. Lu, C.P., Li, G., Mao, J., Wang, L.M., Andrei, E.Y.: Bandgap, mid-gap states, and gating effects in MoS_2. Nano Lett. **14**, 4628–4633 (2014)
13. Gao, J., et al.: Aging of transition metal dichalcogenide monolayers. ACS Nano **10**, 2628–2635 (2016)
14. Budania, P., et al.: Long-term stability of mechanically exfoliated MoS_2 flakes. MRS Commun. **7**, 813–818 (2017)
15. Walter, T.N., Kwok, F., Simchi, H., Aldosari, H.M., Mohney, S.E.: Oxidation and oxidative vapor-phase etching of few-layer MoS_2. J. Vac. Sci. Technol. B **35**, 021203 (2017)
16. Khare, H.S., Burris, D.L.: Surface and subsurface contributions of oxidation and moisture to room temperature friction of molybdenum disulfide. Tribol. Lett. **53**, 329–336 (2014)
17. Khare, H.S., Burris, D.L.: The effects of environmental water and oxygen on the temperature-dependent friction of sputtered molybdenum disulfide. Tribol. Lett. **52**, 485–493 (2013)
18. Ross, S., Sussman, A.: Surface oxidation of molybdenum disulfide. J. Phys. Chem. **59**, 889–892 (1955)
19. Haltner, A.J., Oliver, C.S.: Effect of water vapor on friction of molybdenum disulfide. Ind. Eng. Chem. Fundam. **5**, 348–355 (1966)
20. Pardee, R.P.: The effect of humidity on low-load frictional properties of a bonded solid film lubricant. A S L E Trans. **15**, 130–142 (1972)
21. Pope, L.E., Panitz, J.K.G.: The effects of hertzian stress and test atmosphere on the friction coefficients of MoS_2 coatings. Surf. Coat. Technol. **36**, 341–350 (1988)
22. Stewart, T.B., Fleischauer, P.D.: Chemistry of sputtered molybdenum disulfide films. Inorg. Chem. **21**, 2426–2431 (1982)
23. Serpini, E., et al.: The role of humidity and oxygen on MoS_2 thin films deposited by RF PVD magnetron sputtering. Surf. Coat. Technol. **319**, 345–352 (2017)
24. Pritchard, C., Midgley, J.W.: The effect of humidity on the friction and life of unbonded molybdenum disulphide films. Wear **13**, 39–50 (1969)
25. Johnston, R.M., Moore, A.J.W.: Water adsorption on molybdenum disulfide containing surface contaminants. J. Phys. Chem. **68**, 3399–3406 (1964)
26. Uemura, M., Saito, K., Nakao, K.: A mechanism of vapor effect on friction coefficient of molybdenum disulfide. Tribol. Trans. **33**, 551–556 (1990)
27. Holinski, R., Gänsheimer, J.: A study of the lubricating mechanism of molybdenum disulfide. Wear **19**, 329–342 (1972)
28. Zhao, X., Perry, S.S.: The role of water in modifying friction within MoS_2 sliding interfaces. ACS Appl. Mater. Interfaces **2**, 1444–1448 (2010)
29. Curry, J.F., et al.: Highly oriented MoS_2 coatings: tribology and environmental stability. Tribol. Lett. **64**, 11 (2016)
30. Tran-Khac, B.-C., Kim, H.-J., DelRio, F.W., Chung, K.-H.: Operational and environmental conditions regulate the frictional behavior of two-dimensional materials. Appl. Surf. Sci. **483**, 34–44 (2019)
31. Zhao, X., Zhang, G., Wang, L., Xue, Q.: The tribological mechanism of MoS_2 film under different humidity. Tribol. Lett. **65**, 64 (2017)
32. Lancaster, J.K.: A review of the influence of environmental humidity and water on friction, lubrication and wear. Tribol. Int. **23**, 371–389 (1990)
33. Levita, G., Righi, M.C.: Effects of water intercalation and tribochemistry on MoS_2 lubricity: an ab initio molecular dynamics investigation. ChemPhysChem (2017). https://doi.org/10.1002/cphc.201601143
34. Sresht, V., et al.: Quantitative modeling of MoS_2–solvent interfaces: predicting contact angles and exfoliation performance using molecular dynamics. J. Phys. Chem. C **121**, 9022–9031 (2017)
35. Chow, P.K., et al.: Wetting of mono and few-layered WS_2 and MoS_2 films supported on Si/SiO_2 substrates. ACS Nano **9**, 3023–3031 (2015)
36. Kozbial, A., Gong, X., Liu, H., Li, L.: Understanding the intrinsic water wettability of molybdenum disulfide (MoS_2). Langmuir **31**, 8429–8435 (2015)
37. Luan, B., Zhou, R.: Wettability and friction of water on a MoS_2 nanosheet. Appl. Phys. Lett. **108**, 131601 (2016)
38. Lince, J.R., Loewenthal, S.H., Clark, C.S.: Tribological and chemical effects of long term humid air exposure on sputter-deposited nanocomposite MoS_2 coatings. Wear **432–433**, 202935 (2019)

39. Afanasiev, P., Lorentz, C.: Oxidation of nanodispersed MoS_2 in ambient air: the products and the mechanistic steps. J. Phys. Chem. C **123**, 7486–7494 (2019)
40. Arif, T., Yadav, S., Colas, G., Singh, C.V., Filleter, T.: Understanding the independent and interdependent role of water and oxidation on the tribology of ultrathin molybdenum disulfide (MoS_2). Adv. Mater. Interfaces **6**, 1901246 (2019)
41. Krick, B.A., Vail, J.R., Persson, B.N.J., Sawyer, W.G.: Optical in situ micro tribometer for analysis of real contact area for contact mechanics, adhesion, and sliding experiments. Tribol. Lett. **45**, 185–194 (2011)
42. Colbert, R.S., et al.: Uncertainty in pin-on-disk wear volume measurements using surface scanning techniques. Tribol. Lett. **42**, 129–131 (2011)
43. Burris, D.L., Sawyer, W.G.: Addressing practical challenges of low friction coefficient measurements. Tribol. Lett. **35**, 17–23 (2009)
44. Vasenkov, A., et al.: Reactive molecular dynamics study of Mo-based alloys under high-pressure, high-temperature conditions. J. Appl. Phys. **112**, 013511 (2012)
45. Curry, J.F., et al.: Impact of microstructure on MoS_2 oxidation and friction. ACS Appl. Mater. Interfaces **9**, 28019–28026 (2017)
46. Kresse, G., Joubert, D.: From ultrasoft pseudopotentials to the projector augmented-wave method. Phys. Rev. B **59**, 1758–1775 (1999)
47. Kresse, G., Furthmüller, J.: Efficient iterative schemes for ab initio total-energy calculations using a plane-wave basis set. Phys. Rev. B **54**, 11169–11186 (1996)
48. Perdew, J.P., Burke, K., Ernzerhof, M.: Generalized gradient approximation made simple. Phys. Rev. Lett. **77**, 3865–3868 (1996)
49. Grimme, S., Ehrlich, S., Goerigk, L.: Effect of the damping function in dispersion corrected density functional theory. J. Comput. Chem. **32**, 1456–1465 (2011)
50. Grimme, S., Antony, J., Ehrlich, S., Krieg, H.: A consistent and accurate ab initio parametrization of density functional dispersion correction (DFT-D) for the 94 elements H-Pu. J. Chem. Phys. **132**, 154104 (2010)
51. Monkhorst, H.J., Pack, J.D.: Special points for Brillouin-zone integrations. Phys. Rev. B **13**, 5188–5192 (1976)
52. Larsen, A.H., et al.: The atomic simulation environment—a Python library for working with atoms. J. Phys. Condens. Matter **29**, 273002 (2017)
53. Walsh, A., Catlow, C.R.A.: Structure, stability and work functions of the low index surfaces of pure indium oxide and Sn-doped indium oxide (ITO) from density functional theory. J. Mater. Chem. **20**, 10438–10444 (2010)
54. Miyahara, Y., Grütter, P.: Dissipation modulated kelvin probe force microscopy method. In: Sadewasser, S., Glatzel, T. (eds.) Kelvin Probe Force Microscopy: From Single Charge Detection to Device Characterization, pp. 23–47. Springer, New York (2018)
55. Melios, C., et al.: Carrier type inversion in quasi-free standing graphene: studies of local electronic and structural properties. Sci. Rep. **5**, 10505 (2015)
56. Berg, M., et al.: Layer dependence of the electronic band alignment of few-layer MoS_2 on SiO_2 measured using photoemission electron microscopy. Phys. Rev. B **95**, 235406 (2017)
57. Yi, Y., Lyon, J.E., Beerbom, M.M., Schlaf, R.: Characterization of indium tin oxide surfaces and interfaces using low intensity x-ray photoemission spectroscopy. J. Appl. Phys. **100**, 093719 (2006)
58. Singer, I.L., Bolster, R.N., Wegand, J., Fayeulle, S., Stupp, B.C.: Hertzian stress contribution to low friction behavior of thin MoS_2 coatings. Appl. Phys. Lett. **57**, 995–997 (1990)
59. Gul, A., Bacaksiz, C., Unsal, E., Akbali, B.: Theoretical and experimental investigation of conjugation of 1, 6-hexanedithiol on MoS_2. Mater. Res. **5**(3), 036415 (2018)
60. Costa-Amaral, R., Forhat, A., Caturello, N.A.M.S., Silva, J.L.F.D.: Unveiling the adsorption properties of 3d, 4d, and 5d metal adatoms on the MoS_2 monolayer: a DFT-D3 investigation. Surf. Sci. **701**, 121700 (2020)
61. Scharf, T.W., Goeke, R.S., Kotula, P.G., Prasad, S.V.: Synthesis of Au–MoS_2 nanocomposites: thermal and friction-induced changes to the structure. ACS Appl. Mater. Interfaces **5**, 11762–11767 (2013)
62. Hu, J.J., et al.: Transmission electron microscopy analysis of Mo–W–S–Se film sliding contact obtained by using focused ion beam microscope and in situ microtribometer. Tribol. Lett. **32**, 49–57 (2008)
63. Tagawa, M., et al.: Space environmental effects on MoS_2 and diamond-like carbon lubricating films: atomic oxygen-induced erosion and its effect on tribological properties. Surf. Coat. Technol. **202**, 1003–1010 (2007)
64. Hong, J., et al.: Exploring atomic defects in molybdenum disulphide monolayers. Nat. Commun. **6**, 6293 (2015)
65. Vancsó, P., et al.: The intrinsic defect structure of exfoliated MoS_2 single layers revealed by Scanning Tunneling Microscopy. Sci. Rep. **6**, 29726 (2016)
66. Fleischauer, P.D.: Fundamental aspects of the electronic structure, materials properties and lubrication performance of sputtered MoS_2 films. Thin Solid Films **154**, 309–322 (1987)
67. Lince, J.R., Fleischauer, P.D.: Crystallinity of rf-sputtered MoS_2 films. J. Mater. Res. **2**, 827–838 (1987)
68. Blanco, É., Afanasiev, P., Berhault, G., Uzio, D., Loridant, S.: Resonance Raman spectroscopy as a probe of the crystallite size of MoS_2 nanoparticles. C. R. Chim. **19**, 1310–1314 (2016)
69. Austin, D., et al.: Laser writing of electronic circuitry in thin film molybdenum disulfide: a transformative manufacturing approach. Mater. Today (2020). https://doi.org/10.1016/j.mattod.2020.09.036
70. Schauble, K., et al.: Uncovering the effects of metal contacts on monolayer MoS_2. ACS Nano **14**, 14798–14808 (2020)
71. Shakya, J., Kumar, S., Kanjilal, D., Mohanty, T.: Work function modulation of molybdenum disulfide nanosheets by introducing systematic lattice strain. Sci. Rep. **7**, 9576 (2017)
72. Kröger, M., et al.: Role of the deep-lying electronic states of MoO_3 in the enhancement of hole-injection in organic thin films. Appl. Phys. Lett. **95**, 251 (2009)
73. Irfan, et al.: Energy level evolution of air and oxygen exposed molybdenum trioxide films. Appl. Phys. Lett. **96**, 116 (2010)
74. Ochedowski, O., et al.: Effect of contaminations and surface preparation on the work function of single layer MoS_2. Beilstein J. Nanotechnol. **5**, 291–297 (2014)
75. Choi, S., Shaolin, Z., Yang, W.: Layer-number-dependent work function of MoS_2 nanoflakes. J. Korean Phys. Soc. **64**, 1550–1555 (2014)
76. Moore, D., et al.: Uncovering topographically hidden features in 2D $MoSe_2$ with correlated potential and optical nanoprobes. npj D Mater. Appl. **4**, 1–7 (2020)
77. Hao, G., et al.: Electrostatic properties of few-layer MoS_2 films. AIP Adv. **3**, 042125 (2013)